PHYSICAL REVIEW E **84**, 056304 (2011)

Two interacting cylinders in cross flow

Md. Mahbub Alam[*] and J. P. Meyer

Department of Mechanical and Aeronautical Engineering, University of Pretoria, Pretoria 0002, South Africa

(Received 26 April 2011; revised manuscript received 12 August 2011; published 9 November 2011)

Cylindrical structures in a group are frequently seen on land and in the ocean. Mutual flow interaction between the structures makes the wake very excited or tranquil depending on the spacing between the structures. The excited wake-enhancing forces in some cases cause a catastrophic failure of the structures. This paper presents results of an experimental investigation of Strouhal number (St), time-mean, and fluctuating forces on, and flow structures around, two identical circular cylinders at stagger angle $\alpha = 0^\circ$–180° and gap-spacing ratio $T/D = 0.1$–5, where T is the gap width between the cylinders, and D is the diameter of a cylinder. While forces were measured using a load cell, St was from spectral analysis of fluctuating pressures measured on the side surfaces of the cylinders. A flow visualization test was conducted to observe flow structures around the cylinders. Based on forces, St, and flow structures, 19 distinct flow categories in the ranges of α and T/D investigated are observed, including one quadristable flow, three kinds of tristable flows, and four kinds of bistable flows. The quadristable, tristable, and bistable flows ensue from instabilities of the gap flow, shear layers, vortices, separation bubbles, and wakes, engendering a strong jump or drop in forces and St of the cylinders. The two cylinders interact with each other in six different mechanisms, namely interaction between boundary layer and cylinder, shear layer or wake and cylinder, shear layer and shear layer, vortex and cylinder, vortex and shear layer, and vortex and vortex. While the interaction between vortex and cylinder results in a very high fluctuating drag, that between vortex and shear layer results in a high fluctuating lift. On the other hand, the interaction between shear layer or wake and cylinder weakens mean and fluctuating forces and flow unsteadiness. A mutual discussion of forces, St, and flow structures is presented in this paper.

DOI: 10.1103/PhysRevE.84.056304 PACS number(s): 47.27.wb, 47.32.cb, 47.32.ck

I. INTRODUCTION

Slender structures in groups have many engineering applications, for example, chimney stacks, tube bundles in heat exchangers, high-rise buildings, harvesting wave and tide energy from the ocean, overhead power-line bundles, bridge piers, stays, masts, chemical-reaction towers, and offshore platforms. Naturally, it is important to understand the proximity effect on aerodynamics associated with multiple closely spaced cylindrical structures. Two fluid-dynamically interfering cylinders may be considered as the basic element of multiple structures and the knowledge of this flow is insightful for understanding the flow around more structures. As such, the flow around two cylinders has received a great deal of attention in the literature. There is no doubt that flow physics around two cylinders is much more complex and complicated than that around a single cylinder, because of interference between the cylinders, between the wakes, among four shear layers, etc. The alternate shedding of vortices in the near wake leads to fluctuating forces on the structures and may cause structural vibrations, acoustic noise, or resonance, which in some cases can trigger failure. The study of aerodynamics of two closely separated structures is thus of both fundamental and practical significance. Fluid forces, Strouhal numbers (St), and flow structures are the major factors considered in the design of slender structures subjected to a cross flow.

The flow behind two cylinders has been previously classified based on T/D and α. See Fig. 1(a) for the definitions of the symbols. A number of approaches have been used to classify the fluid behavior of circular cylinders. Based on the interference effect between the two cylinders, Zdravkovich [1] divided the whole region of possible arrangements of two cylinders into four: (i) the proximity interference region, where the flow around one cylinder affects the other; (ii) the wake interference region—the near-wake flow of the upstream cylinder is unaffected by the downstream one; however, the downstream one is significantly affected by the upstream cylinder; (iii) the proximity and wake interference region, where both proximity and wake interference are significant; (iv) the no-interference region, where the wake of one cylinder does not affect the other. Sumner *et al.* [2] conducted flow visualization and particle image velocimetry (PIV) measurements for $T/D = 1.0$–5.0, $\alpha = 0^\circ$–90° and Reynolds number Re = 850–1900 ($\mathrm{Re} = U_\infty D/\nu$, where U_∞ is the free-stream velocity and ν is the kinematic viscosity), and divided the T/D-α plane into three: (1) the single-body flow regime, $T/D = 1.0$–1.125 and $\alpha = 0^\circ$–90°, where two cylinders act like an isolated body with a single vortex-shedding frequency; (2) the small incidence angle regime, $T/D > 1.125$ and $\alpha = 0^\circ$–20°, where shear layer reattachment or the impingement of vortices onto the downstream cylinder takes place; (3) the large incidence angle regime, $T/D = 1.125$, $\alpha = 20^\circ$–90°, where vortex pairing, splitting, enveloping, and synchronizing occur. Gu and Sun [3] measured the time-averaged pressure on two cylinders ($T/D = 0.1$–2.5 and $\alpha = 0^\circ$–90°), and observed three distinct pressure distributions, viz., patterns I_B, II_B, III_B, on the downstream cylinder, which occurred over $\alpha = 0^\circ$–9.65°, 9.7°–15°, and 16°–90°, respectively, at $T/D = 0.7$. The downstream cylinder was completely and partially submerged in the wake of the other, respectively, in patterns I_B and II_B but not in pattern III_B. All these

---

[*] alamm28@yahoo.com

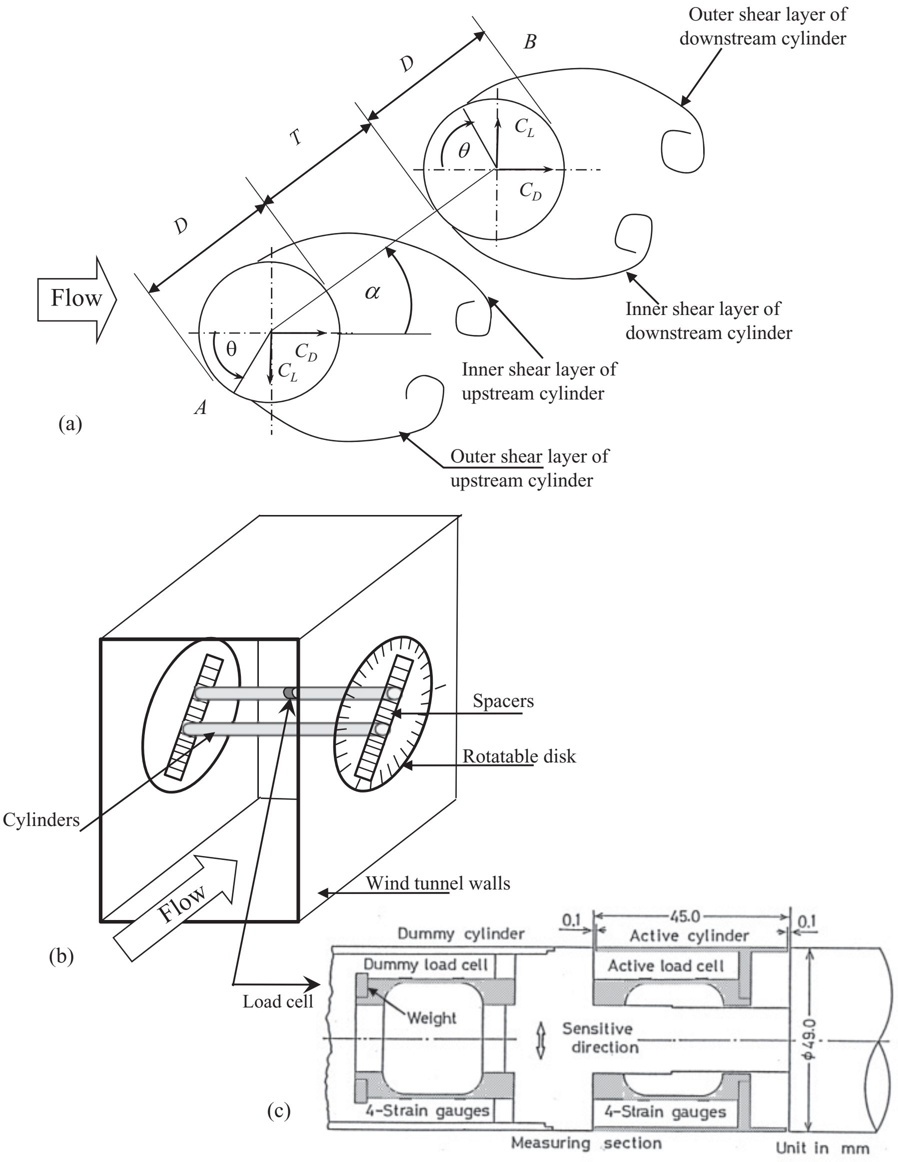

FIG. 1. (a) Notation of staggered configuration, (b) a schematic of experimental arrangement, (c) load cell details.

classifications are useful from the engineering design point of view, though they do not provide detailed information on forces and the flow structure around the cylinders. The flow classifications mentioned above were based on near-wake flow structures. Little is known about what happens in the far wake regarding vortex or wake coupling and three-dimensional interactions of vertical structures. Even for a single cylinder, the two rows of alternating vortices in the near-wake interact and transform into two near-parallel shear layers followed by a second wake characterized by a frequency lower than the near wake [4–6]. The distance between the cylinder and the second wake decreases with increase in Re consistently with $\mathrm{Re}^{-1/2}$ power law for the range of Re = 50–800 [6]. The features were in light of the two-dimensional aspects. Three-dimensional interactions are much more complex. For two side-by-side cylinders, four rows of vortices prevail depending on T/D and α. Therefore more parameters are involved in the interaction. The present paper incorporates near-wake, quasi-two-dimensional flow characteristics.

Time-mean drag and lift forces acting on two staggered cylinders have been examined in literature [7–16], with most of the emphasis being on the downstream cylinder. Only a few studies have reported force measurements for the upstream cylinder [3,17–20]. Furthermore, fluctuating force measurements in the literature are very scant, though the fluctuating lift and drag forces acting on structures are a major cause of the fatigue failure of the structures and are used for predicting flow-induced responses. The noteworthy features of mean force data observed were "inner-lift peak" at smaller α and T/D where the cylinders are near in line, and "outer-lift peak" at a larger α and T/D [21]. A number of different explanations for the origin of the inner- and outer-lift peaks have been explored in the literature, which were summarized in Ting *et al.* [22]. Recent experiments by Alam *et al.* [20], involving mean and fluctuating force measurements, pressure measurements, surface oil-flow visualization, and conventional flow visualization, have provided more physical insight into the origin of the inner- and outer-lift peaks. They presented and discussed their results with variation in T/D,

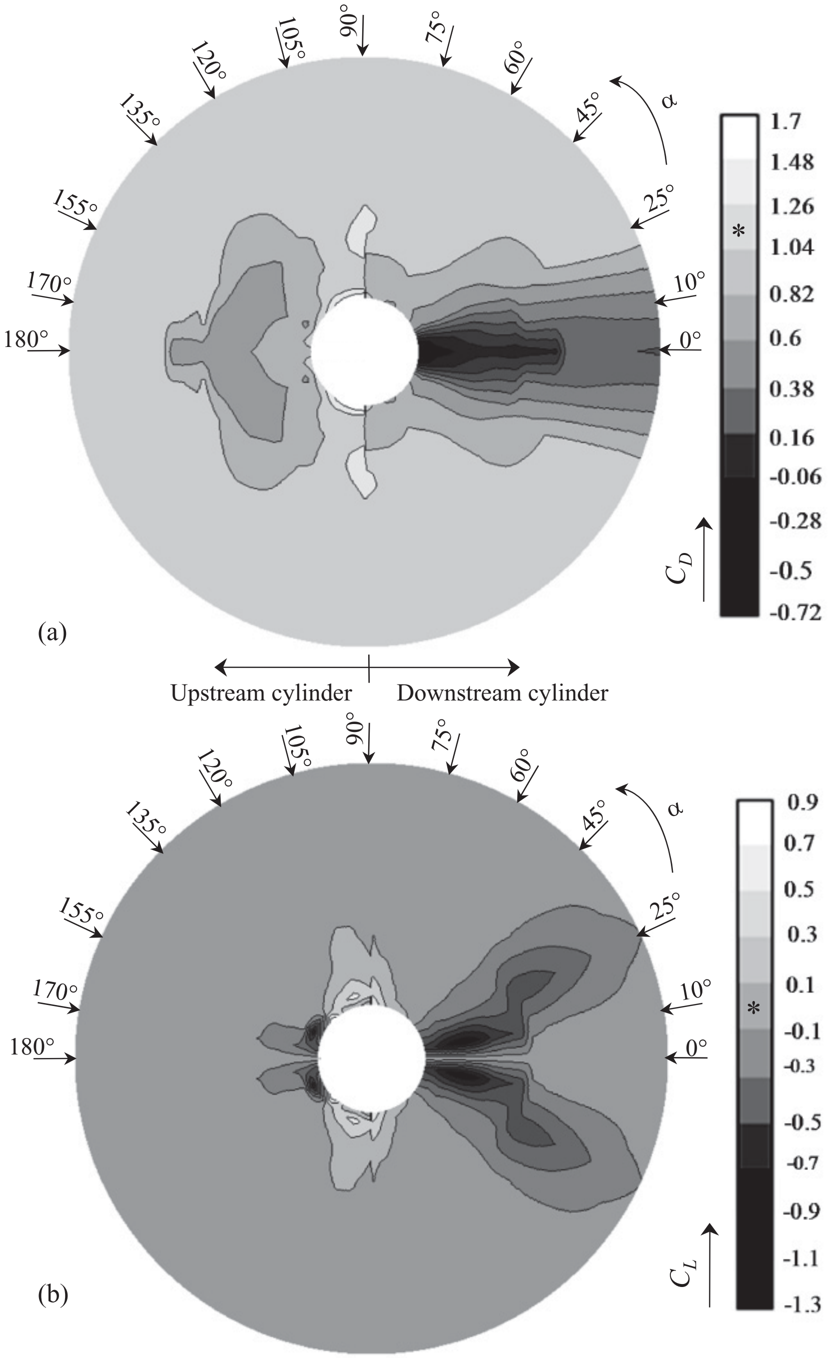

FIG. 2. Contour maps of (a) time-mean drag coefficient C_D and (b) time-mean lift coefficient C_L. Points marked by asterisk denote values of coefficients of an isolated cylinder.

failing to explicate global features of flow with variations of both T/D and α and to classify flow regime globally. Most literature sources are connected to one of the three arrangements, tandem ($\alpha = 0^\circ$), side-by-side ($\alpha = 90^\circ$), or staggered ($0^\circ < \alpha < 90^\circ$). Furthermore, flow classifications in the literature are based on either theoretical treatment [1,11] or experimental measurement of forces, St, and pressure [10,17,23–28] or flow visualization image [29–31]. Determining the fluid dynamics from measured quantities is prone to misinterpretation, particularly when done without the benefit of accompanying flow visualization. Articles with both measured quantities and flow visualization are very few [26,27,32]. The present study measures all possible quantities including mean and fluctuating forces, St, and pressure. Flow visualization and surface oil-flow techniques are also employed to get insight into the physical flow around the cylinders and to get a better understanding of the mean and fluctuating forces and St.

The objectives of this study were (i) to classify the flow regime globally based on forces, St, and flow structures, (ii) to elucidate the flow structure for each regime, (iii) to find possible interaction mechanisms, and (iv) to make a correlative discussion of flow, forces, and St, for the whole range of $\alpha = 0^\circ$–180° and $T/D = 0.1$–5.0. Another objective of the study was to find possible discontinuities and the respective instabilities responsible in the whole range. To this end, a fine resolution in T/D was adopted, $\triangle T/D = 0.1$ for $T/D = 0.1$–1.2, $\triangle T/D = 0.3$ for $T/D = 1.2$–3.0, and $\triangle T/D = 0.5$

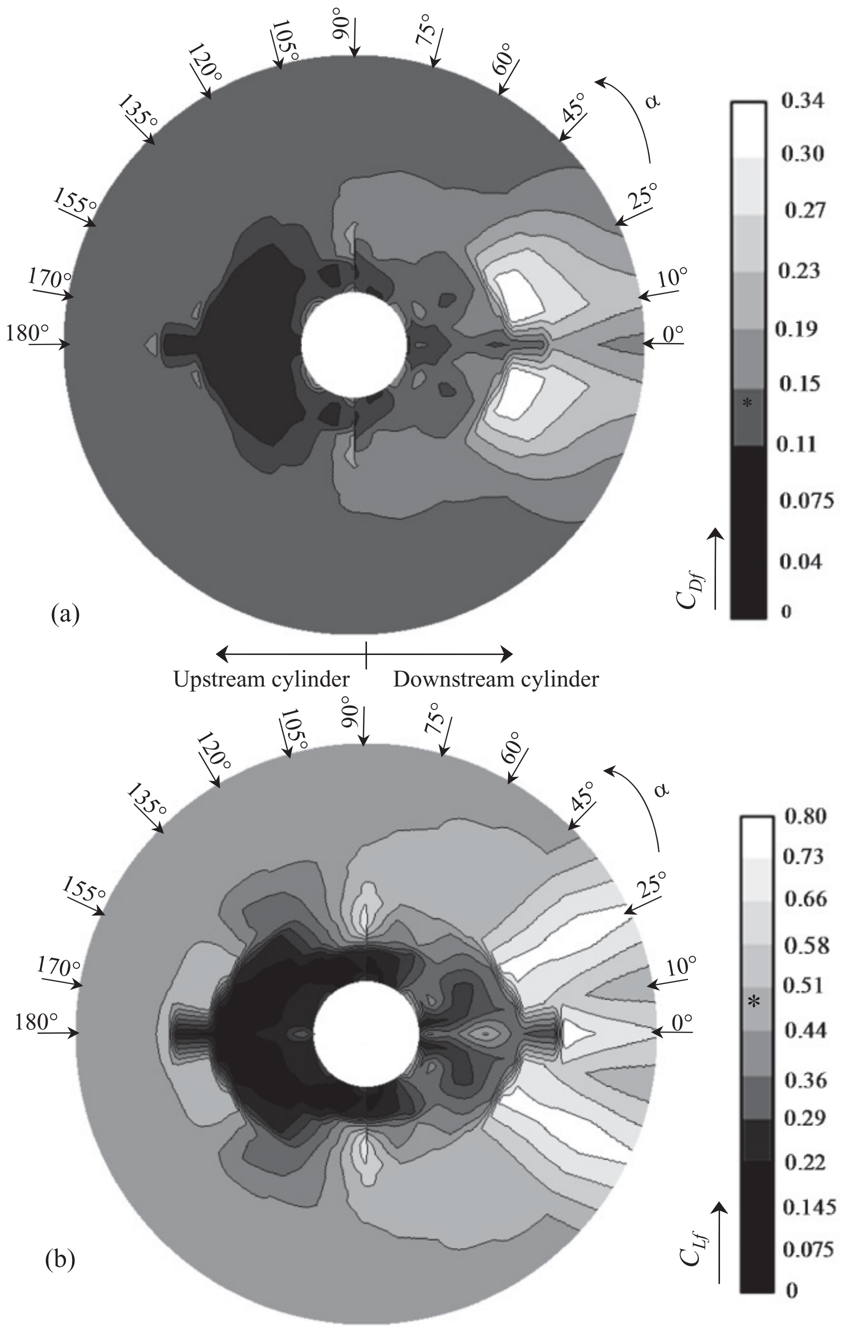

FIG. 3. Contour maps of (a) fluctuating (rms) drag coefficient C_{Df} and (b) fluctuating (rms) lift coefficient C_{Lf}. Points marked by asterisk denote values of coefficients of an isolated cylinder.

for $T/D = 3.0$–5.0. The linkage between force and flow structure and possible interactions is discussed in detail.

II. EXPERIMENTAL DETAILS

Experiments were conducted at the fluid mechanics laboratory of Kitami Institute of Technology, Japan. Measurements were done in a low-speed, closed-circuit wind tunnel with a test section of 1.20 m in height, 0.30 m in width, and 2.2 m in length [Fig. 1(b)]. Fluid forces, St, and cylinder-surface pressure measurements and surface oil-flow visualization were conducted in this wind tunnel at a Re of 5.52×10^4 based on the diameter of a single cylinder. In the test section side walls, two circular holes of 0.5 m diameter, one opposite to the other, were made where two circular disks, each including a slit for cylinders, marked 0°–360° with a resolution of 1°, were placed [Fig. 1(b)]. The disks were rotatable to adjust the stagger angle. The diameter of each cylinder was 49 mm. The cylinders spanned the horizontal 0.3-m dimension of the wind tunnel. The turbulent intensity was 0.5%. A fine-mesh honeycomb that was placed at the entrance of the test section to provide a uniform flow was responsible for such turbulence. In order to check the spanwise uniformity of flow as well as the spanwise separation of flow over a single cylinder for fluid forces being measured by a load cell (which will be discussed next), circumferential time-averaged and fluctuating pressures on the surface of the cylinder at the midsection, and at ±35 mm and ±80 mm (from the midsection), were measured. The results showed that the time-averaged and fluctuating pressure distributions at the five different sections were the same within

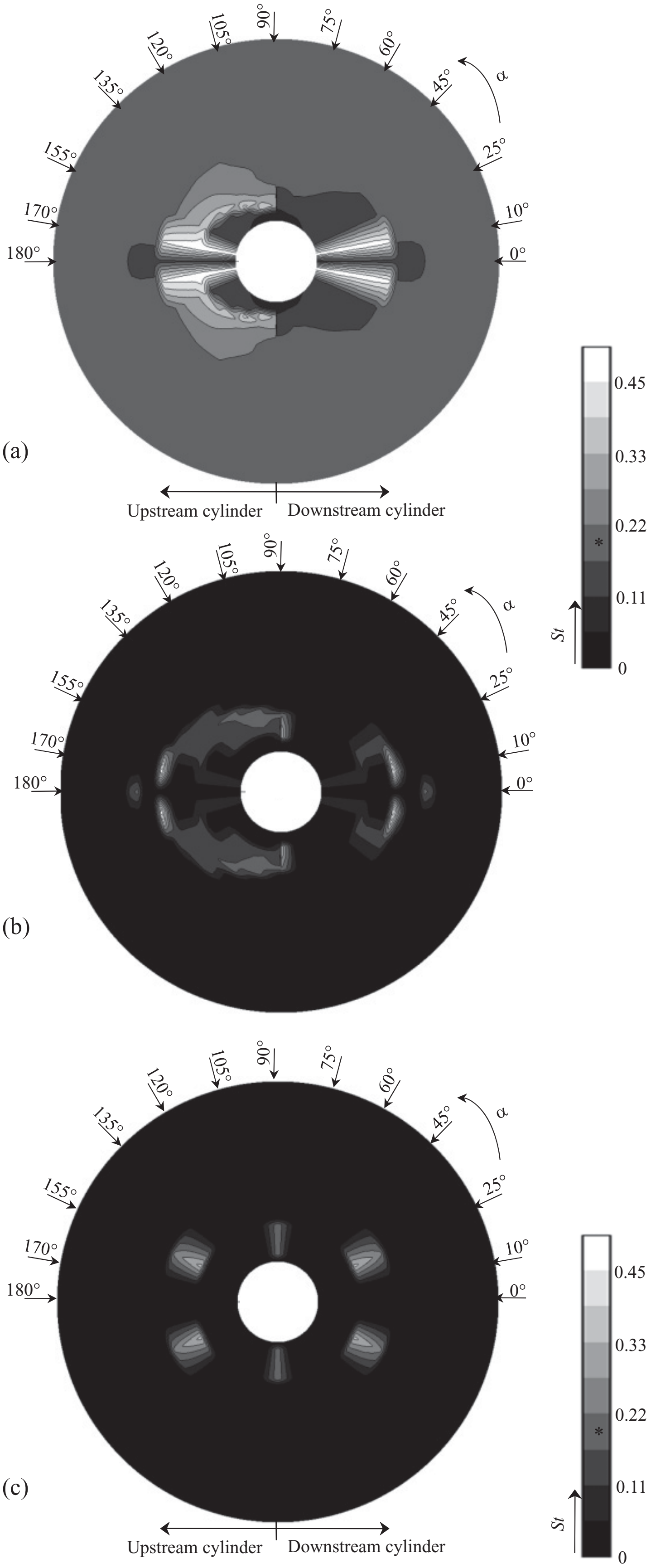

FIG. 4. Contour maps of Strouhal number (St). (a) Primary mode, (b) secondary mode, (c) tertiary mode. Point marked by asterisk denotes St value of an isolated cylinder.

the accuracy of measurement. The geometric blockage ratio was 4% based on a single cylinder; total blockage for the cylinder pair was 8%. Based on their measurements, West and Apelt [33] suggested that the blockage had virtually no effect on forces if <6% and could have a very small effect if between 6 and 9%. Therefore, the present blockage (8%) is expected to have a negligible effect on C_D. The cylinder aspect ratio at the test section was 6.1. West and Apelt [34] established that the forces on an elemental section are independent of spanwise location for aspect ratios >10; i.e., "long" cylinder conditions occur. From the results published by Szepessy and Bearman [35], it was found that the force was ∼3% higher for an aspect ratio of 6 than that for the aspect ratio of 10. More details of the tunnel and blockage and aspect ratio effects are given in Alam *et al.* [18,20].

Fluid forces were measured over a small spanwise length of the cylinders, using load cells [Fig. 1(c)]. The cylinder to be measured was built in with an active ("live") section of a spanwise 45-mm ($0.92D$) length and two dummy sections. This size was determined taking into account the cross-correlation length of fluctuating pressure in the spanwise direction of the cylinder. The active section, placed between the two dummy sections, corresponded to the midspan of the cylinder and was installed with a load cell that consisted of four semiconductor strain gauges. One of the dummy sections was also instrumented with another load cell of the same configuration. The load cell inside the active section measured a combination of fluid forces and forces due to vibration transmitted from outside through the cylinder support, while that inside the dummy section measured the latter forces only. Hence the fluid forces acting on the active section could be calculated by subtracting the output of the load cell inside the dummy section from that of the load cell inside the active section. See Sakamoto and Oiwake [36] or Sakamoto *et al.* [37] or Alam *et al.* [20] for details of the load cell. Since multiple flow modes may occur and their switch appears rather random, the force signals may jump suddenly and are nonstationary. However, the signals may be considered to be stationary within each mode; that is, we may determine the averaged and fluctuating force coefficients for individual modes. A conditional sampling technique was deployed for this task. See Alam *et al.* [18] for more details of this technique.

St was estimated from spectral analysis of the fluctuating pressures measured on the side surfaces of the cylinders. Figure 1 is a schematic diagram showing the arrangement of two cylinders, definition of symbols, and coordinate systems. The stagger angle α is defined as the angle between the free-stream flow and the line connecting the centers of the two cylinders. T is the gap width between the cylinders, as opposed to center-to-center spacing adopted by other researchers. In this study, the repulsive (outward-directed) lift force is considered to be positive and the attractive (inward-directed) lift force is considered to be negative. The position of a point on the surface of a cylinder is defined by the azimuth angle θ, measured from the direction of free-stream flow. θ is considered to be 0°–180° for the outer surfaces and 180°–360° for the inner surfaces of the cylinders. The cylinder A is tentatively assumed to be fixed, and traversing of the cylinder B can be done with variation of the two parameters T/D and α. Experiments were performed for $\alpha = 0^\circ, 10^\circ, 25^\circ, 45^\circ, 60^\circ, 75^\circ, 90^\circ, 105^\circ, 120^\circ, 135^\circ, 155^\circ, 170^\circ$, and 180°, for the spacing ratio of $T/D = 0.1$–5. Very-fine tuning of T/D was adopted with $T/D = 0.1$, 0.2, 0.3, 0.5, 0.6, 0.7, 0.8, 0.9, 1.1, 1.2, 1.5, 1.8, 2.1, 2.4, 2.7, 3.0, 3.5, 4.0, 4.5, and 5.0.

Two semiconductor pressure transducers (Toyoda PD104K) located at the midsection of the two cylinders, respectively, were used to measure cylinder surface pressure. The transducers responded reasonably well to the pressure fluctuations up to 500 Hz with a gain factor of 1 ± 0.06, with a negligible phase lag. This frequency was well above the frequency of vortex shedding from the cylinders. Details of the pressure transducer have been given in Alam *et al.* [20].

Flow visualization was carried out in a water channel with a 250 × 350 mm working section and 1.5 m in length. A fine-mesh honeycomb was used to remove any large-scale irregularities. Two circular tubes with identical diameters of 20 mm were used. The Reynolds number in the water channel experiment was 350. This Reynolds number is beyond the transition range to turbulent in wake, as fully turbulent shedding conditions prevail for $\mathrm{Re} > 300$ [38]. The flow was visualized by using the hydrogen bubble technique, involving a platinum wire of 0.02 mm in diameter.

Surface oil-film techniques were used to confirm the flow pattern on the cylinders, especially to have information on reattachment and separation positions of flow on the cylinders. The cylinders were wrapped with a black film of 0.03 mm in thickness, and then an even coating of a solution containing silicone oil, titanium dioxide, oleic acid, and kerosene at a ratio of 45:3:2:2 in weight was applied to the surface. The solution distribution on the cylinder surface was achieved after at least 15 min of exposure to the uniform flow in the wind tunnel. The blackthe film was then unwrapped carefully, and photographs of solution distribution on the film were taken with a digital camera. Surface oil-flow visualizations were performed at the same Reynolds number as the measurements of fluid force and pressure.

III. FLUID FORCES AND STROUHAL NUMBER

Time-averaged drag coefficient (C_D), time-averaged lift coefficient, (C_L), fluctuating drag coefficient (C_Df), and fluctuating lift coefficient (C_{Lf}) are plotted in a T/D-α plane, and then the contour maps are drawn, as shown in Figs. 2 and 3. In the scale bars, the color or the range marked by the asterisk indicates the value of a single isolated cylinder. The result is described with reference to Fig. 1, in which cylinder A is fixed, and traversing of cylinder B is done with variation of the two parameters T/D and α, which suffice to determine the possible arrangement of the two cylinders. It may be noted that cylinder B acts as the downstream and upstream cylinders for $|\alpha| < 90^\circ$ and $|\alpha| > 90^\circ$, respectively, i.e., the left and right sides of the contour map show the values of coefficient of the upstream and downstream cylinders, respectively. At the peripheries of the inner and outer circles, the values of T/D are 0.0 and 5.0, respectively. Note that the values of C_D, C_{Df}, C_L, C_{Lf} and St of a single cylinder are 1.12, 0.14, 0.48, and 0.186, respectively. Repulsive and attractive C_L are considered as positive and negative, respectively (Fig. 1).

The contour maps show that fluid force coefficients in the downstream region briskly change with changes in T/D and α; however, the upstream region retains single cylinder values for $T/D > 3.0$ for any value of α. This signifies that the interference effect of the upstream cylinder on the downstream cylinder is much stronger but the opposite is rather weak. As seen in Fig. 2(a), the upstream cylinder experiences somewhat lower C_D at $|\alpha| > 120^\circ$, $T/D < 3.0$ than a single isolated cylinder. The downstream cylinder experiences highly negative C_D at $|\alpha| < 10^\circ$, $T/D < 3.0$, with a global minimum value of -0.72 at $\alpha = 0^\circ$, $T/D = 0.1$. Maximum C_D of 1.26−1.48 and 1.48−1.7 acts on the cylinder at $\alpha \approx 90^\circ$, $T/D = 1.2-2.0$ and $\alpha = 90^\circ-120^\circ$, $T/D < 0.2$, respectively. While enhanced coupled-vortex shedding is responsible for the higher C_D in the former region, there is perfectly single-body flow for the latter region. $C_L = -1.03$ and -1.15 to -1.25 are the minimum (most negative) values occurring at $|\alpha| = 155^\circ$, $T/D = 0.3$ and $\alpha = 10^\circ$, $T/D = 0.8-1.1$, respectively. C_L becomes maximum of 0.85 at $|\alpha| = 135^\circ$, $T/D = 0.1$.

Significantly higher C_{Lf} and C_{Df} act on the cylinder at $\alpha < 35^\circ$, $T/D < 2.5$ (Fig. 3). While the global maximum value of C_{Lf} is 0.8, 1.58 times the single cylinder value, that of C_{Df} is 0.34, 2.35 times the single cylinder value. On the other hand, C_{Lf} and C_{Df} are extremely small for $|\alpha| > 60^\circ$, $T/D < 3.0$. The observation suggests that the interference effect has not only a negative impact with increasing forces, but also a positive impact with reducing forces on the cylinder. Its impact, however, depends on α and T/D.

Figure 4 shows isocontours of St in T/D-α plane. At some regions where bistable or tristable flows appear, there are more than one St corresponding to the individual flow structures. While Fig. 4(a) displays the primary dominant St, Figs. 4(b) and 4(c) display secondary and tertiary St. Therefore, the highlighted regimes in Figs. 4(b) and 4(c) imply the regimes of the bistable and tristable flow regarding St. The lowest St is 0.06−0.11 at $|\alpha| = 60^\circ-120^\circ$, $T/D < 0.5$ [Fig. 4(a)] and the highest St is 0.45−0.5 at $|\alpha| = 10^\circ$, $T/D < 2.5$ [Fig. 4(a)]. A scrupulous observation on the St map (Fig. 4) unveils that St has a strong relationship with C_D and/or C_L, but less with C_{Lf} or C_{Df}: St is inversely related with C_D and/or C_L. Where C_D or C_L is large in magnitude, St is lower and vice versa.

IV. CLASSIFICATION OF FORCE REGIMES AND FLOW STRUCTURES

In the previous section, variation in C_D, C_L, C_{Df}, C_{Lf}, and St with change in T/D and α has been observed rapid, implying that interference between the two cylinders, between the two wakes, and among four shear layers results in different fluid dynamics around, behind, and between the cylinders depending T/D and α. The interference gives rise to flow separation, recirculation, bubble formation, coupled and quasiperiodic vortices and instabilities of the gap flow, shear layers, and wakes. As a matter of fact, 19 distinct flow regimes have been presently identified as illustrated in Fig. 5, which is sketched based on rigorous observation of Figs. 2–4. The features of each regime are described as follows:

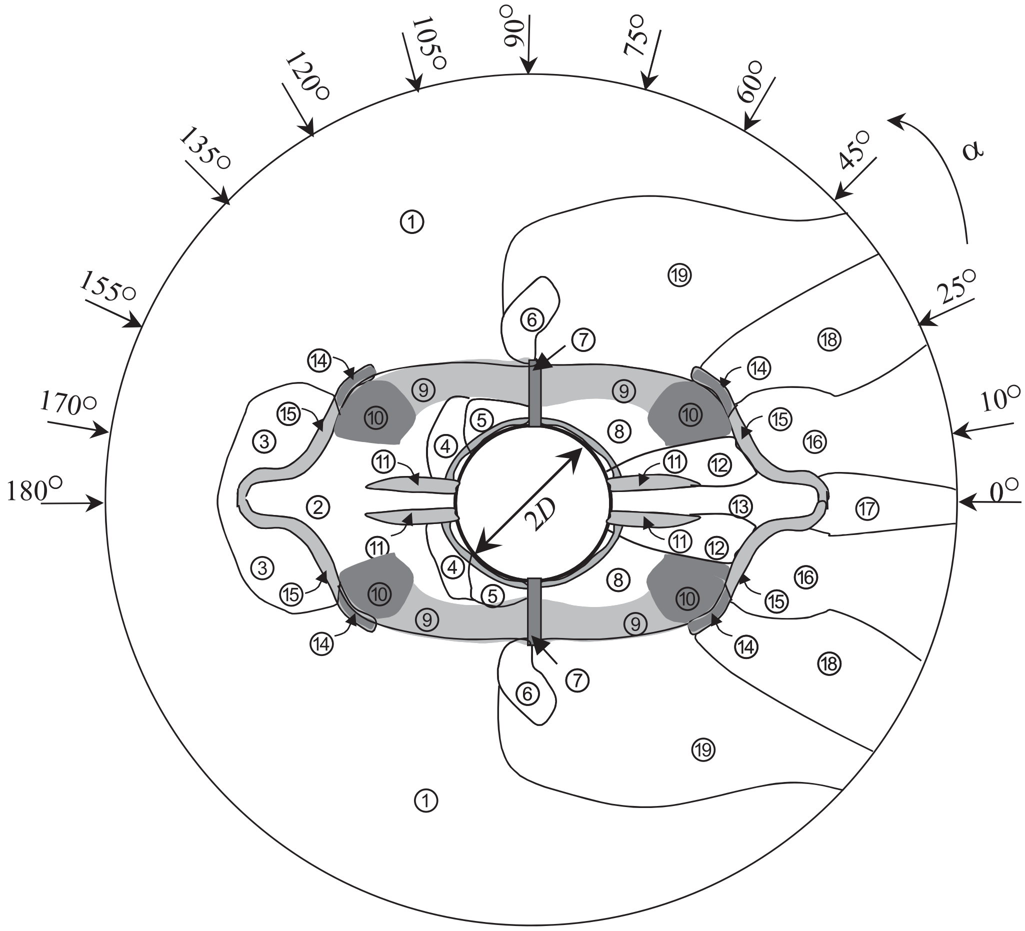

FIG. 5. Sketch specifying various regions. The regions marked by shadows are multistable flow regions.

(1) *No-interference regime*. C_D, C_L, C_{Df}, C_{Lf}, and St are almost the same as those of a single isolated cylinder. At this region, the cylinder is not interfered with by the other.

(2) *Upstream-cylinder vortex-suppressed regime*. Reduced C_D, zero C_L, very low C_{Df} and C_{Lf}, and high St. The low magnitude of forces is attributed to the fact that for $|\alpha| = 170^{\circ}-180^{\circ}$, the downstream cylinder acts as a stabilizer of the upstream cylinder wake propelling the vortex formation [Fig. 6(a_1)], and for the rest $|\alpha|$ ($=150^{\circ}-170^{\circ}$) formation of fully developed Karman vortex behind the upstream cylinder is retarded by the presence of the downstream cylinder [Fig. 6(a_2)]. The high St is due to a retreat of vortex formation length [Fig. 6(a_1)]. In general, forces (particularly C_D) and St are inversely correlated [39,40].

(3) *Excited upstream-cylinder flow regime*. Somewhat increased C_{Df} and C_{Lf}, due to appearance of fully developed Karman wake and enhanced rolling of the upstream-cylinder shear layers. The downstream cylinder barring the shear layers thrusts them to roll strongly [Fig. 6(b)].

(4) *Highly deflected gap flow regime*. Attractive (negative) C_L, low C_{Lf}, and low St. Highly deflected gap flow towards the upstream cylinder wake causes attractive C_L [Fig. 6(c)], providing anticlockwise circulation around the cylinder. No Karman vortex shedding just behind the upstream cylinder results in the low C_{Lf}. The two cylinders behave like a single body, forming a single wake with alternating Karman vortex, hence corresponding to a low St. This regime includes a bistable flow regime marked by a shadow. Intermittent formation [Fig. 6(c_2)] and burst [Fig. 6(c_3)] of separation bubble on the gap-side surface of the upstream cylinder cause such a bistable flow being responsible for a large difference in C_L on the upstream cylinder. However, St values for both cases were the same, because the outer shear layers of the cylinders mainly govern the vortex shedding. Intermittent formation and burst were not observable in visualization because of the low Re (=350), but were observed in force and pressure measurements (Re = 5.52×10^4). See Ref. [20] for the details of the bistable flow.

(5) *Perfectly single-body regime*. Very high C_D, repulsive (positive) high C_L, low C_{Lf} and C_{Df}, and low St. The two cylinders act as a single bluff body, resulting in a high C_D and low St [Fig. 6(d)]. Stagnation point on the cylinders shifts towards the gap side and a lower pressure gradient prevails on the gap-side surface of the upstream cylinder. Both contribute to the repulsive C_L. The lower gradient of pressure occurs due to retardation of flow through the gap by the inner-front quadrant surface of the downstream cylinder. This regime also incorporates a bistable flow regime marked by a shadow. A turbulent reattachment and detachment of the inner-shear layer of the upstream cylinder initiate the bistable flow. Typical lift force signal showing the bistable nature of flow at $T/D = 0.13$ is presented in Fig. 7. Note that while only a stable reattached flow was observed at $T/D \leqslant 0.10$, only a detached flow was observed at $T/D \geqslant 0.20$. In order

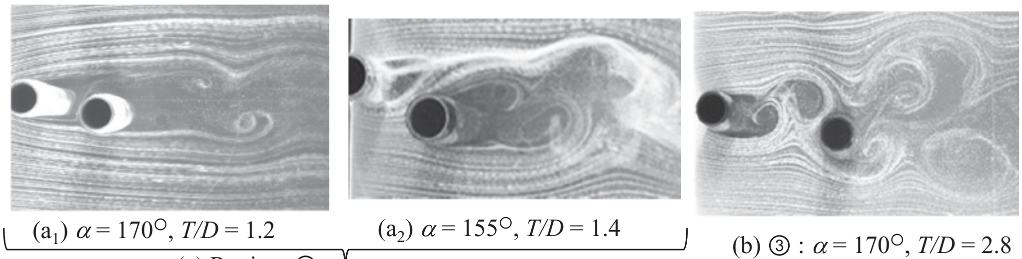
(a_1) $\alpha = 170^{\circ}$, $T/D = 1.2$

(a_2) $\alpha = 155^{\circ}$, $T/D = 1.4$

(a) Regime ②

(b) ③ : $\alpha = 170^{\circ}$, $T/D = 2.8$

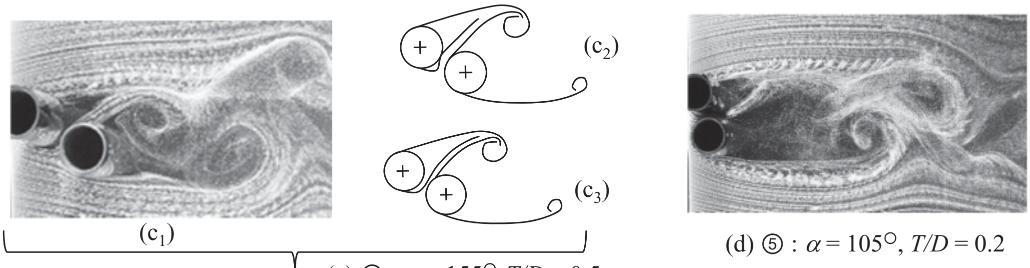

(c_1)

(c) ④ : $\alpha = 155^{\circ}$, $T/D = 0.5$

(d) ⑤ : $\alpha = 105^{\circ}$, $T/D = 0.2$


(e) ⑥ : $\alpha = 90^{\circ}$, $T/D = 1.3$

FIG. 6. (*Continued*)

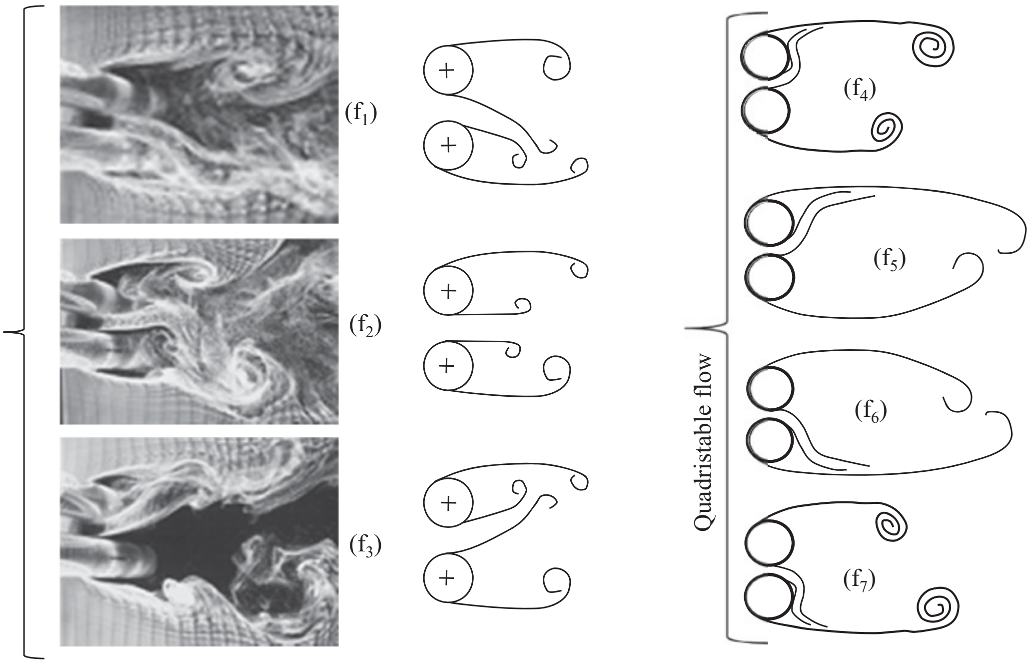

(f) ⑦ : f_1 - f_3, tristable flow, $\alpha = 90^\circ$, $T/D = 0.4$; f_4 - f_7, quadristable flow, $T/D = 0.13$.

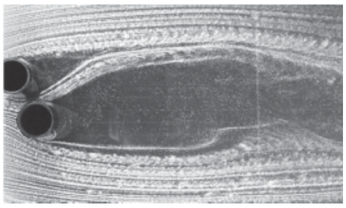

(g) ⑧ : $\alpha = 75^\circ$, $T/D = 0.5$

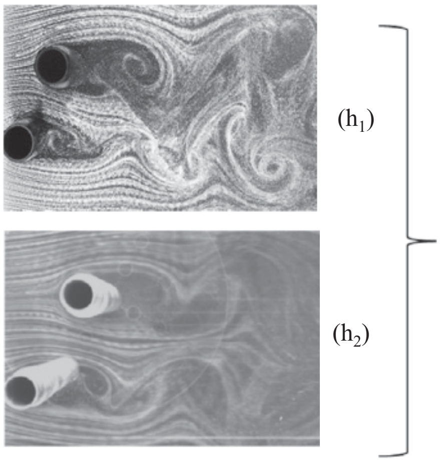

(h) ⑨ : Bistable flow at $\alpha = 60^\circ$, $T/D = 1.2$

FIG. 6. (*Continued*)

to have insight into the reattachment and detachment of the inner-shear layer, time-averaged pressure (C_p) distributions and surface oil-flow patterns together with sketches of flow patterns for $T/D = 0.10$ and 0.20 are shown in Figs. 8 and 9. The oil-flow patterns for $T/D = 0.10$ and 0.20 indicate the appearance of two different flow patterns at these spacings. As is evidenced by pressure distribution and surface oil-flow patterns for $T/D = 0.10$, the stagnation point on the upstream cylinder is at $\theta = 348^\circ$ (Fig. 8) and the flow on the inner-front quadrant ($\theta = 348^\circ - 270^\circ$) surface of the upstream cylinder is somewhat retarded by the front surface downstream cylinder, causing a smaller pressure gradient on the inner-front quadrant (Fig. 9). The inner-shear layer of the upstream cylinder separates turbulently at $\theta = 180^\circ$ followed by a turbulent reattachment at $\theta = 135^\circ$ (Fig. 8). The eventual separation of the shear layer occurs at $\theta = 110^\circ$. For $T/D = 0.20$, laminar separation of the gap flow from the surfaces of the upstream and the downstream cylinders occurs at $\theta = 248^\circ$ and -78°, respectively. The occurrence of turbulent reattachment and detachment of the inner-shear layer of the upstream cylinder differentiates the two flow patterns for $T/D = 0.10$ and 0.20. Thus, the bistable flow is owing to intermittent turbulent reattachment and detachment of the inner-shear layer of the upstream cylinder.

(6) *Antiphase vortex-shedding regime*. Very high C_D, repulsive C_L, high C_{Df} and C_{Lf}. Vortex shedding from one cylinder is constantly coupled with that from the other in an antiphase fashion, with their frequencies identical, which is referred to as antiphase vortex shedding. The antiphase shedding fortifying the Karman vortices is highly coherent, responsible for the

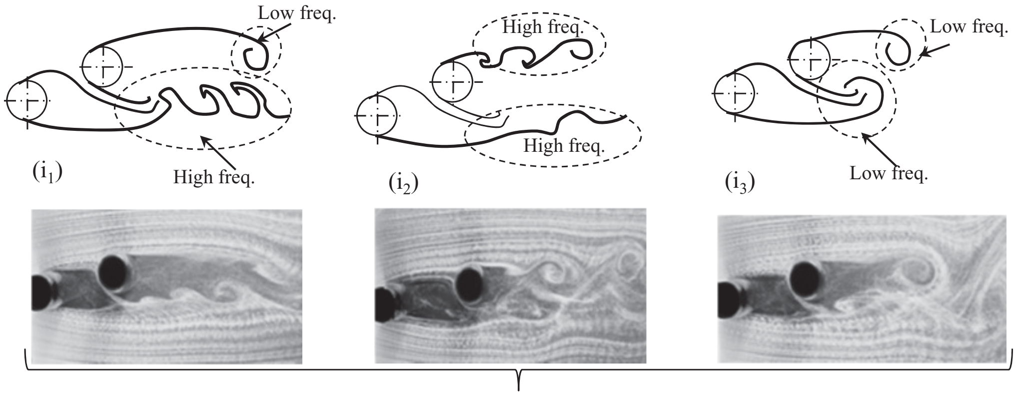

(i) ⑩ : Tristable flow, $\alpha = 20^\circ$, $T/D = 1.5$

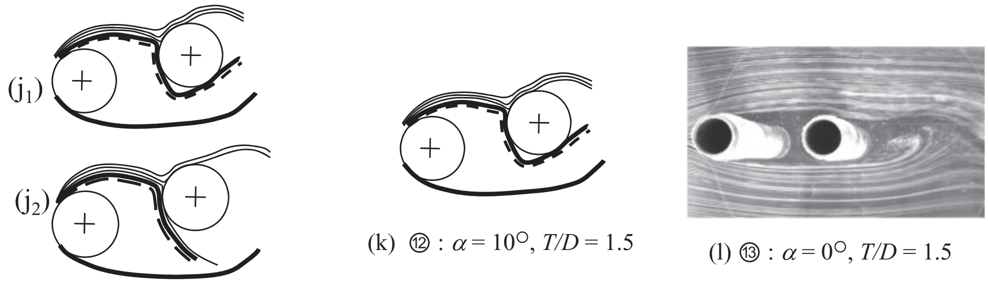

(j) ⑪ : Bistable flow $\alpha = 10^\circ$, $T/D = 1.0$

(k) ⑫ : $\alpha = 10^\circ$, $T/D = 1.5$

(l) ⑬ : $\alpha = 0^\circ$, $T/D = 1.5$

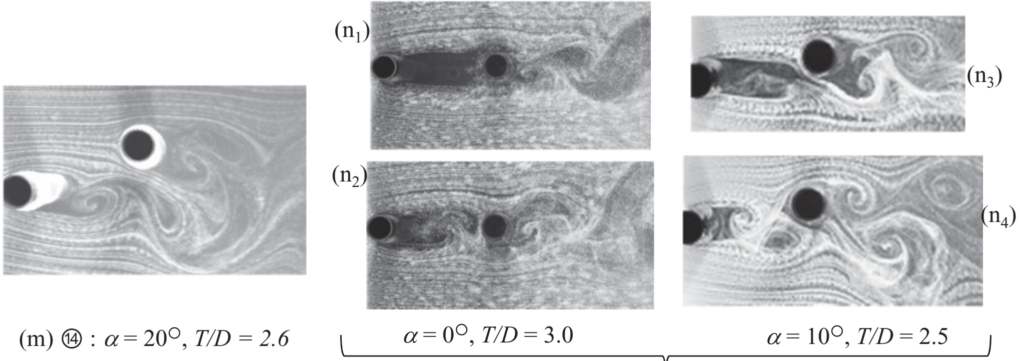

(m) ⑭ : $\alpha = 20^\circ$, $T/D = 2.6$

$\alpha = 0^\circ$, $T/D = 3.0$ $\alpha = 10^\circ$, $T/D = 2.5$

(n) ⑮: Bistable flow

FIG. 6. (*Continued*)

high C_D, C_{Df}, and C_{Lf} [Fig. 6(e)]. A predominance of antiphase shedding was also observed by Kamemoto [23], Williamson [32], Peschard and Le Gal [31], Kolar *et al.* [41], and Meneghini *et al.* [42]. Also, for two square cylinders in a side-by-side arrangement, Alam *et al.* [43] observed highly correlated antiphased vortex shedding which resulted in a high C_D, C_{Df}, and C_{Lf}. In this region strong coupling between the two side-by-side wakes prevails. Peschard and Le Gal [31] provided a theoretical model using two coupled Landau equations for the two side-by-side wakes. The model was able to extract most of the experimental features including antiphase and in-phase locked states, and asymmetric bistable locked states.

(7) *Tristable and quadristable flip-flopping flow regime.* Three modes of flow, considering the upper cylinder, associated with wider wake, symmetric wake, and narrow wake, are generated and switched from one to another [Figs. 6(f$_1$)–6(f$_3$)]. The corresponding St observed are low [Fig. 4(a), $\alpha < 90^\circ$], intermediate [Fig. 4(c), $\alpha = 90^\circ$], and high [Fig. 4(b), $\alpha > 90^\circ$], respectively. The three St maps [Figs. 4(a)–4(c)] indeed reflect the view that the side-by-side arrangement ($\alpha = 90^\circ$) is the critical geometry between two staggered configurations of $\alpha < 90^\circ$ and $\alpha > 90^\circ$. For $\alpha < 90^\circ$ (say $\alpha = 85^\circ$), the gap flow is away from the upper cylinder (wide wake) corresponding to the lower St [Fig. 4(a)]; for $\alpha > 90^\circ$ (say $\alpha = 95^\circ$), the gap flow biases toward the upper cylinder (narrow wake) corresponding to the higher St [Fig. 4(a)]. $\alpha = 90^\circ$ should correspond to a symmetric wake (nonbiased gap flow) with intermediate St [Fig. 4(c)]. Hence, for $\alpha < 90^\circ$ or $\alpha < 90^\circ$, the three flow modes appear intermittently, switching from one

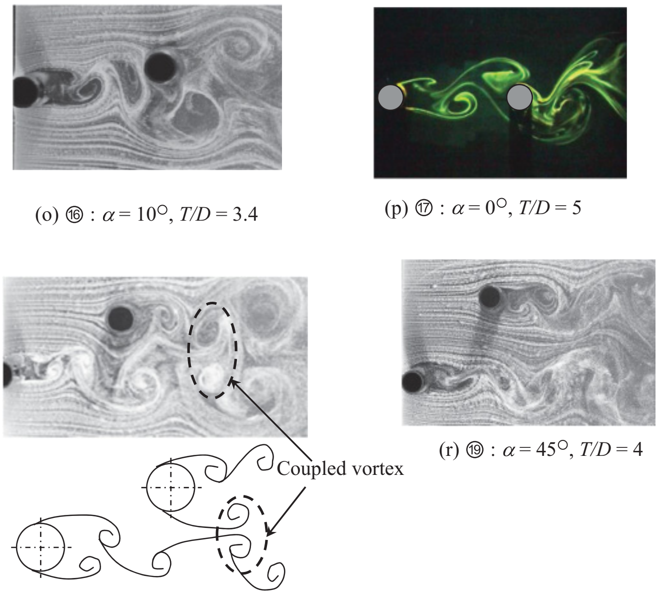
(o) ⑯ : $\alpha = 10^\circ$, $T/D = 3.4$

(p) ⑰ : $\alpha = 0^\circ$, $T/D = 5$

(r) ⑲ : $\alpha = 45^\circ$, $T/D = 4$

(q) ⑱ : $\alpha = 25^\circ$, $T/D = 3.4$

FIG. 6. (Color online) Representative flow structures at different regions. (a)–(r) See text for details. (f) Ref. [18]; (j), (n) Ref. [20].

to another. Thus the tristable flow ensues from instability of the gap flow, appearing at $T/D = 0.2$–1.2. This regime includes a quadristable flow appearing at $T/D = 0.1$–0.2, caused by simultaneous instabilities of the gap flow and a separation bubble [Figs. 6(f_4)–6(f_7)]. The gap flow biasing towards the upper cylinder forms a separation bubble on the rear surface [Fig. 6(f_4)]. The bubble is unstable; hence it bursts. After the burst, the gap flow may remain on the same side [Fig. 6(f_5)] or veer to the other side again generating a bubble [Fig. 6(f_7)] or not [Fig. 6(f_6)]. Typical lift force signal shown in Fig. 10 illustrates more details.

(8) *Single-body-like regime*. Reduced C_D, C_{Df}, and C_{Lf}, and a single low St in either wake. The two cylinders behave like a single body, giving a larger effective bluff width, generating weak vortex shedding from the two outer sides of the cylinders [Fig. 6(g)]. Thus a single low St persists in the wake. The gap flow acting as a base bleed postpones the shear layers' rolling, hence reducing C_D, C_{Df}, and C_{Lf}.

(9) *Wake lock-in bistable flow regime*. Reduced C_D, C_{Df}, and $C_L f$, and two and one St values for the upstream- and downstream-cylinder wakes, respectively [Figs. 4(a) and 4(b)]. Generally, the upstream-cylinder wake being narrow generates vortices at a higher frequency than the downstream cylinder [Fig. 6(h_1)]. Since the two wakes are in close proximity, the upstream-cylinder wake locks in to that of the downstream cylinder [Fig. 6(h_2)], generating vortices at the frequency of the downstream-cylinder wake, i.e., the two wakes are locked in. The lock-in occurs intermittently, with a flow switching from Figs. 6(h_1) to Fig. 6(h_2) and vice versa. Therefore, the upstream cylinder generates vortices at two St (the low and high), while the downstream cylinder generates vortices at one St (the low) [Figs. 4(a) and 4(b)].

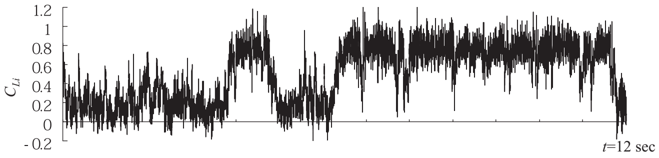

FIG. 7. Lift force signal of the upstream cylinder for $\alpha = 105^\circ$, $T/D = 0.13$, indicating bistable nature of flow [20].

(10) *Shear-layer-lock-in tristable flow regime*. Curtailed C_D, C_{Df}, and C_{Lf}, and two St values for the upstream and downstream cylinders. Three modes of flow with regard to vortex-shedding frequencies appear intermittently. They are (i) the flow with a high St for the gap flow and the outer-shear layer of the upstream cylinder and a low St for the outer-shear layer of the downstream cylinder [Figs. 4(a) and 6(i_1)]; (ii) the flow with a high St for both cylinders [Figs. 4(b) and 6(i_2)]: lock-in of the downstream-cylinder shear layers to the upstream ones; and (iii) the flow with a low St for both cylinders: lock-in of the upstream-cylinder shear layers to the downstream ones [Figs. 4(c) and 6(i_3)]. Alam and Sakamoto [44] observed the tristable flow in the cross-wavelet analysis results of two simultaneously acquired pressure signals on the two cylinders. However, they failed to provide detailed flow structures. How the lock-in of the shear layers is initiated is of great interest. Consider as a reference the flow pattern in which the gap flow and the outer-shear layer of the upstream cylinder shed vortices at the high frequency and the outer-shear layer of the downstream cylinder at the low frequency [Fig. 6(i_1)]. In the reference flow pattern, since the gap flow and the outer-shear layer of the downstream cylinder shed vortices at higher and lower frequencies, respectively, there may be a tendency for the gap flow and the shear layer to shed vortices in alternating fashion at the same frequency. To shed vortices in alternating fashion, (a) the gap flow may induce the outer-shear layer to be modified to shed vortices at the higher frequency, and (b) the outer-shear layer may induce the gap flow to be modified to shed vortices at the lower frequency. Now in the first case, when the outer-shear layer is modified to shed vortices at the higher frequency, all the shear layers including those through the gap of the two cylinders shed vortices at the same frequency [higher frequency, Fig. 6(i_2)], which has been termed as the lock-in of the downstream-cylinder shear layer to the upstream one. In the second case, the gap flow is modified to shed vortices at the lower frequency and induces the outer-shear layer of the upstream cylinder to shed vortices at the same frequency [Fig. 6(i_3)]. Thus now all the shear layers shed vortices at the lower frequency, which has been termed as the lock-in of the upstream-cylinder shear layer to the downstream one. Thus the tristable flow is caused by instabilities of the shear layers.

(11) *Bubble-burst bistable flow regime*. Highly negative C_L (-1.21). The bistable flow results from intermittent formation and burst of a separation bubble formed on the inner-side surface of the downstream cylinder [Fig. 6(j)]. The mode in which the separation bubble persists results in a highly negative C_L. This regime is characterized by a negative lift peak known as "inner-lift peak regime" [8–10,17]. The researchers observed rapid changes in the mean lift force for small adjustments to the geometry, which was attributed to the high-speed flow deflected through the gap between the cylinders. The explanation was not so specific, hence later

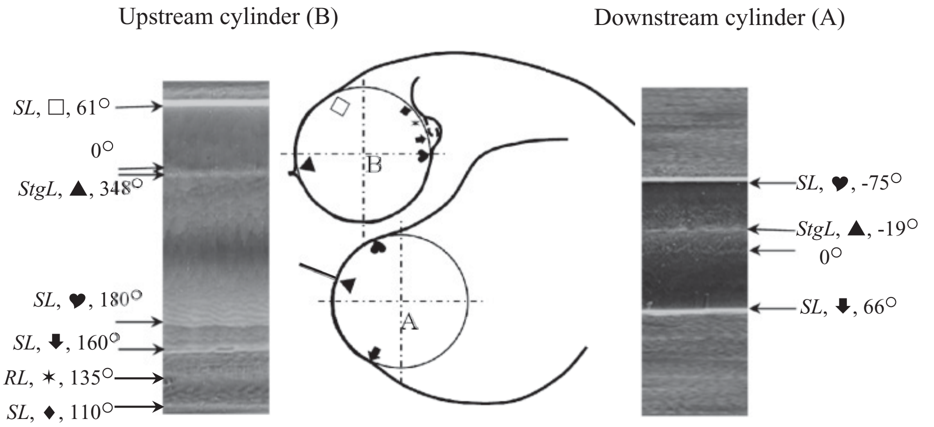

(a) $T/D = 0.10$

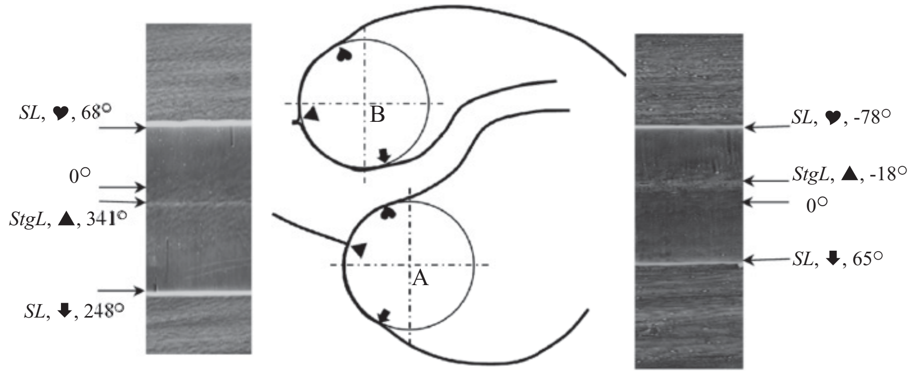

(b) $T/D = 0.20$

FIG. 8. Surface oil-flow patterns and corresponding sketches of flow for $\alpha = 105^\circ$. SL: separation line; StgL: stagnation line; RL: reattachment line.

Alam *et al*. [20] with pressure measurement and surface oil-flow results showed that the lift peak is mainly due to a separation bubble forming on the inner side of the cylinder and the rapid change in mean lift is connected to the formation and burst of the separation bubble. In fact the global minimum C_L (-1.21) occurs at this regime. Since only one wake is formed behind the cylinders, St of the two cylinders in a mode is the same, a high (St $\approx$ 0.47) and low (St $\approx$ 0.09) for the modes with and without bubbles, respectively [Figs. 4(a) and 4(b)]. Such a kind of bistable flow was also detected by Gu and Sun [3]. The two modes were consistent with patterns II_B and III_B, respectively, defined by Gu and Sun [3].

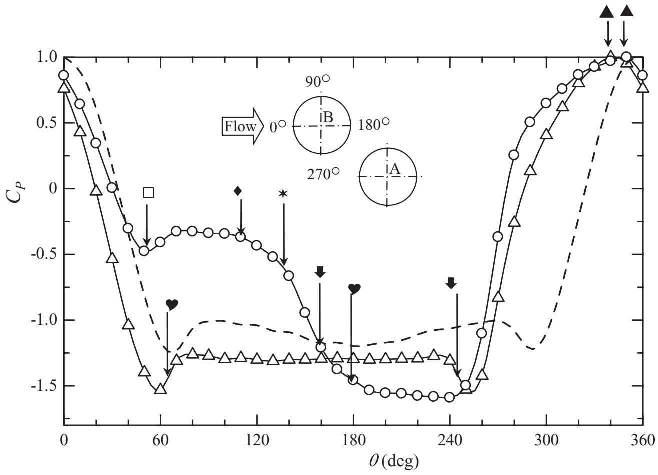

FIG. 9. Time-averaged pressure coefficient distributions on the surface of the upstream cylinder (B) for $\alpha = 105^\circ$: circles: $T/D = 0.10$; triangles: $T/D = 0.20$ (regime 5); dotted line: single isolated cylinder. For definitions of other symbols, see Fig. 8.

(12) *Separation-bubble flow regime*. Attractive C_L, and high St, resulting from a separation bubble formed [Fig. 6(k)]. The flow structure is similar to the separation-bubble mode [Fig. 6(j_1)] appearing in regime 11. Therefore, St is very high and C_L is still negative.

(13) *Fully submerged flow regime*. Zero C_L and highly negative C_D. The downstream cylinder is fully submerged in the wake of the upstream cylinder [Fig. 6(l)]. The most negative C_D of -0.72 happens in this regime.

(14) *Vortex-triggered tristable flow regime*. The upstream-cylinder wake is generally narrow and the downstream one is wide, corresponding to a high and low St, respectively. The convective vortices from the upstream cylinder sometimes trigger the vortex shedding from the downstream cylinder, forcing the downstream cylinder to shed vortices at the higher St. The three modes of flow are (i) the flow with a higher and lower St for the upstream and downstream cylinders, respectively; (ii) the flow with the higher St for both cylinders; and (iii) the flow with synchronized St approximately equal to that of a single cylinder. The first and second modes with a thicker flow through the gap resemble those [Figs. 6(i_1) and 6(i_2)] in regime 10. The third mode is given in Fig. 6(m).

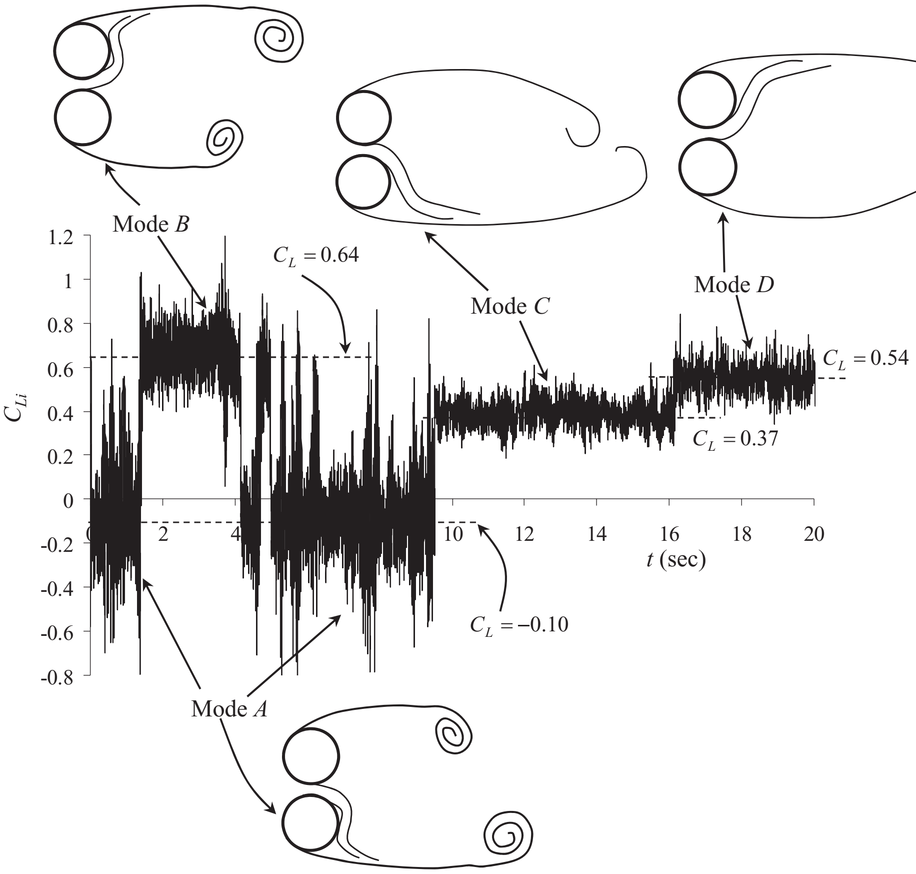

FIG. 10. Time history of instantaneous lift force on the lower cylinder at $T/d = 0.13$ and flow sketches corresponding to the different modes of lift force [56].

This regime is in fact a transition regime in which fully developed flow behind the upstream cylinder starts to form. Therefore, a jump in fluctuating forces [Figs. 3(a) and 3(b)] and St [Figs. 4(a) and 4(b)] occurs.

(15) *Shear-layer-reattachment bistable flow regime.* Two flow patterns appear alternately. For $\alpha = 0^\circ$, i.e., in-tandem arrangement, the shear layers separating from the upstream cylinder reattach steadily onto the downstream cylinder [Fig. 6(n_1)] or strongly roll up behind the upstream cylinder [Fig. 6(n_2)], and for $0^\circ < \alpha < 25^\circ$, only the inner-shear layer of the upstream cylinder reattaches onto the front surface of the downstream cylinder [Fig. 6(n_3)] or strongly rolls up before it [Fig. 6(n_4)]. While the reattachment mode corresponds to a smaller fluctuating force [Figs. 3(a) and 3(b)] and high St [Fig. 4(a)], the roll-up mode corresponds to a larger fluctuating force [Figs. 3(a) and 3(b)] and St approximately equal to that of a single isolated cylinder.

(16) *Vortex-triggered synchronized shedding regime.* Very high C_{Df}. The inner-shear layer of the upstream cylinder rolls just before the front surface of the downstream cylinder [Fig. 6(o)], causing a higher fluctuation of pressure on the front surface, hence, a higher C_{Df} on the downstream cylinder. Though the downstream cylinder confronts a highly turbulent nonuniform approaching flow, its vortex-shedding frequency is the same as that of the upstream cylinder confronting a smooth uniform approaching flow. This happens due to the fact that the convective alternating vortices from the upstream cylinder trigger the vortex shedding of the downstream cylinder.

(17) *Coshedding flow regime.* Very high C_{Lf}. It is engendered by an alternating buffeting of the upstream-cylinder vortices convective along the side surfaces of the downstream cylinder [Fig. 6(p)].

(18) *Synchronized coupled-vortex regime.* Extremely high C_{Lf} and attractive C_L. The inner-shear layer of the downstream cylinder sheds vortices in synchronization with the convective inner vortices from the upstream cylinder, generating a coupled vortex, resulting in a higher fluctuating pressure on the inner-side surface of the downstream cylinder, hence the cylinder experiences a higher C_{Lf} [Fig. 6(q)]. C_L measurement results by Zdravkovich and Pridden [10] showed that C_L is minimum at $\alpha \approx 25^\circ$, $T/D = 1$–4. The maximum C_{Lf} in this regime is $\sim$0.8.

(19) *Small interference regime.* Somewhat high C_{Df} and C_{Lf}; the downstream cylinder is outside the wake of the upstream cylinder; hence the interference effect is trivial [Fig. 6(r)].

V. PHYSICAL INTERACTIONS

A single cylinder in cross flow in general generates boundary layers, shear layers, alternating vortices, and wake. When two cylinders are in close proximity, boundary layers, shear

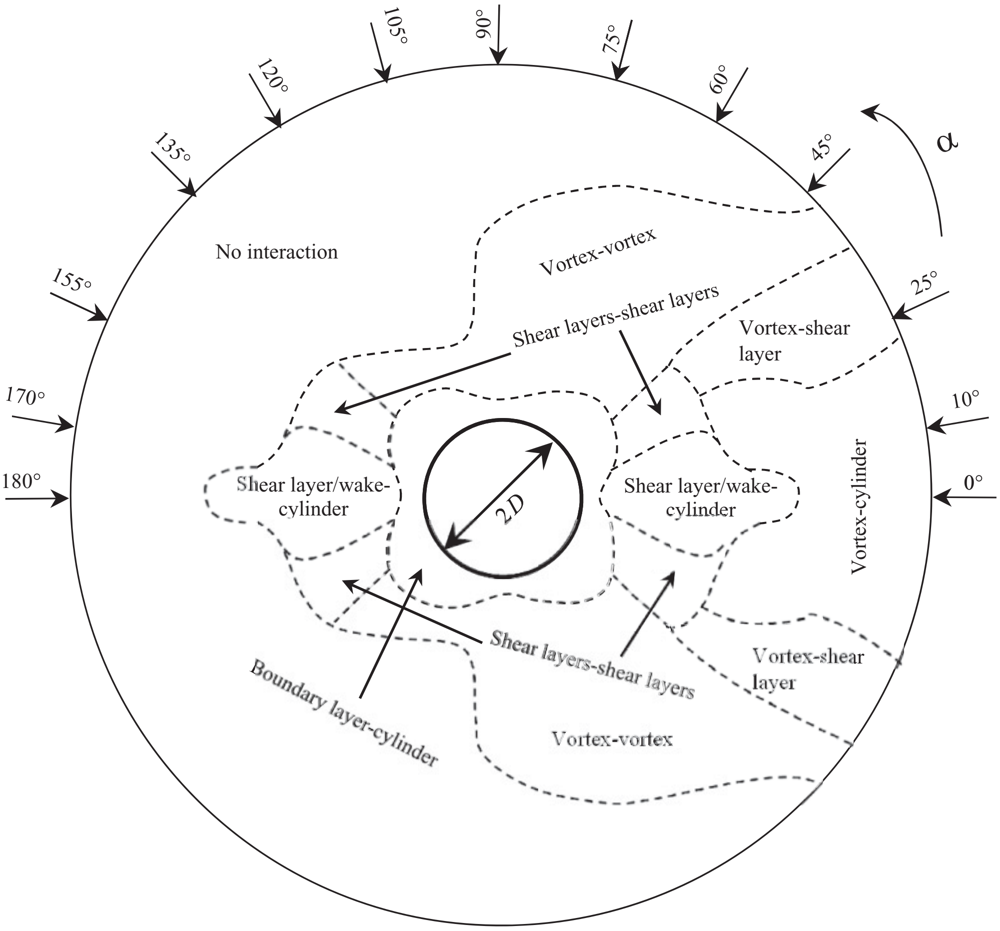

FIG. 11. Possible interactions and their regimes in T/D-α plane.

layer, vortex, and wake are therefore four physical interacting parameters. A scrupulous observation of flow structures in Fig. 6 and the flow structure details in Sec. IV reveals the interactions of the six types. They are interaction between (i) boundary layer and cylinder, (ii) shear layer or wake and cylinder, (iii) shear layer and shear layer, (iv) vortex and cylinder, (v) vortex and shear layer, and (vi) vortex and vortex. Their regimes are given in Fig. 11. Naturally, their boundaries include more than one flow type described in Sec. IV. The details of the interactions are given as follows.

Boundary layer and cylinder interaction. This interaction occurs when T/D is small, i.e., $T/D < 0.3$–0.6 depending on α. Interacting with the other cylinder, the boundary layer of a cylinder may form separation bubbles, delay to separate, reattach, etc. See Figs. 6(c) 6(d), 6(f), 6(g), and 8. The interaction therefore intensifies C_D and C_L but weakens C_{Df} and C_{Lf}. The two cylinders being very close behave like a combined cylinder.

Shear layer or wake and cylinder interaction. This happens when a shear layer(s) from one cylinder interacts on the other cylinder surface by reattaching, impinging, forming a separation bubble, etc. [Figs. 6(j)–6(l), 6(n_1), and 6(n_3)]. Naturally, one of the cylinders is completely [Figs. 6(l) and 6(n_1)] or partially [Figs. 6(j), 6(k), and 6(n_3)] submerged in the wake of the other; hence it can also be termed as wake and cylinder interaction. The shear layer interacted upon by the cylinder loses its strength to shed the alternating Karman vortex, hence forces wane significantly. Being completely submerged in the wake of the other, the cylinder acting as a stabilizer suppresses the flow unsteadiness between the cylinders. The interaction occurs when two cylinders are nearly in line, $|\alpha| \approx 0^\circ$–20°, $0.3 < T/D < 2.3 - 3$.

Shear layer and shear layer interaction. Here the shear layer(s) of a cylinder directly interacts with that of the other. The interaction causes intermittent interlock-in of the shear layers, hence generates vortices at more than one frequency [Fig. 6(i)], and reduces forces on the cylinders. Since α of this interaction regime is higher than that of the shear layer or wake and cylinder interaction regime, generation of two shear layers through the gap is possible. The two shear layers interact with themselves and the outer-shear layers [Fig. 6(i)].

Vortex and cylinder interaction. When T/D is greater than the critical spacing of two nearly in-line cylinders, the shear layers of the upstream cylinder cannot reach the downstream cylinder; hence they roll between the cylinders, forming alternate vortices. Thus the alternate vortices from the upstream cylinder strike on the downstream cylinder and embrace the side surface during passing on the cylinder [Figs. 6(o) and 6(p)]. This interaction is generally very strong, intensifying C_{Df} significantly. Gursul and Rockwell [45] investigated the interaction of the oncoming two rows of vortices on an elliptical leading edge and observed very high fluctuating pressure on the surface where the vortices reached.

Vortex and shear layer interaction. For a larger α, the downstream cylinder becomes offset from the inner row of vortices from the upstream cylinder, hence the vortices cannot interact with the downstream cylinder, but can interact with the inner-shear layer. Interacting with the shear layer while it is growing, the vortices force the shear layer to form a synchronized coupled vortex [Fig. 6(q)]. This interaction renders a very high C_{Lf}, as an alternate interaction between vortex and shear layer intervenes.

Vortex and vortex interaction. For a further increase in α, the transverse distance between the cylinders becomes large, hence each cylinder forms a separate wake immediately behind them. The vortices on the two inner rows interact with each other and combine the two wakes into a wider one [Figs. 6(e), 6(f), and 6(r)], which results in a slightly higher C_D, C_{Df}, and C_{Lf}.

VI. FORCE AND FLOW CONTROL MECHANISMS

The above discussion on possible interactions and their effects on forces bears physical insight into force and/or flow control mechanisms. As such, vortex and cylinder or vortex and shear layer interactions intensify forces, while shear layer or wake and cylinder interaction reduces forces and the unsteadiness of the flow. In the literature, aerodynamics and hydrodynamics means for reducing fluid forces are classified into four categories [46,47]:

(a) The control of shear layer by surface protrusion (tripping wire, fin, helical strakes, helical wires, studs, etc.) (e.g., James and Truong [48] and Alam *et al.* [49]), or by placing a small cylinder in the shear layer (e.g., Sakamoto *et al.* [50]; Alam *et al.* [51]).

(b) The control of the entrainment layers by shrouds (perforated gauze, axial rods, etc.), which supply irrotational fluid to the entrainment layers (e.g., Knell [52]).

(c) The instability control of wakes by near-wake stabilizers (splitter plate, guiding plates, etc.) which reduce the interaction of two opposite shear layers (Bearman [53]).

(d) Approaching flow control by placing a small rod in front of the model (e.g., Igarashi and Itoh [54]; Sakamoto *et al.* [55]). Forces reduce when the shear layers from the rod attach to the cylinder.

As seen, categories (a), (c), and (d) belong to the interaction between boundary layer and cylinder or shear layer or wake and cylinder where C_{Df} and C_{Lf} are reduced most. Therefore, the interaction mechanism is the key factor in reducing or enhancing forces or flow unsteadiness.

VII. CONCLUSIONS

Fluid forces, St, and detailed insight into flow structures and their instability are investigated for two circular cylinders of identical diameters for $\alpha = 0^\circ, 10^\circ, 25^\circ, 45^\circ, 60^\circ, 90^\circ, 105^\circ, 75^\circ, 120^\circ, 135^\circ, 155^\circ, 170^\circ$, and 180° and $T/D = 0.1-5.0$. Contour map of forces and St in T/D-α plane were made, providing overall variation of forces, St, and flow structures with changing T/D and α. A mutual discussion of forces, St, and flow structures were given. The investigation leads to the following conclusions.

C_D, C_L, C_{Df}, C_{Lf}, and St of the cylinders are strong functions of α and T/D, connected to 19 distinct flow patterns, including one quadristable flow, three kinds of tristable flows, and four kinds of bistable flows. The quadristable, tristable, or bistable flow engenders strong jumps in C_D, C_L, C_{Df}, C_{Lf}, and St of the cylinders. *Quadristable flow:* This occurs in a side-by-side arrangement at small T/D (=0.1−0.2), resulting from simultaneous instabilities of the gap flow and separation bubble. *Tristable flow:* The three kinds of triastable flows appearing at different regimes have different characteristics. The first kind of tristable flow happening at regime 7 is due to instability of the gap flow forming a narrow wake, wide wake, and symmetric wake. The second kind appearing at regime 10 is caused by lock-in instability of the shear layers, with frequency lock-in of a shear layer to the others. The third kind occurring at regime 14 results from vortex-triggered synchronization. *Bistable flow:* The first kind of the bistable flow appearing at regime 15 is the instability of cylinder shear layers tending to attach or detach to or from the other cylinder. The second kind of bistable flow results from instability of a laminar separation bubble forming and bursting on the cylinder surface, regimes 4 and 11. The third kind of bistable flow is generated from instability of a shear layer susceptible to turbulent reattachment and detachment on the rear surface of the same cylinder, regime 5. The fourth kind of bistable flow results from instability of the two wakes in which the upstream cylinder wake intermittently locks-in to the downstream one with regard to vortex-shedding frequency, regime 9.

Six different interacting mechanisms between the cylinders were observed: boundary layer and cylinder interaction, shear layer or wake and cylinder interaction, shear layer and shear layer interaction, vortex and cylinder interaction, vortex and shear layer interaction, and vortex and vortex interaction. Each of them had different influences on the induced forces and St. There exist two islandlike regimes (regime 16: $\alpha = 10^\circ-25^\circ$, $T/D = 2.2-4.0$; regime 16: $\alpha = 18^\circ-32^\circ$, $T/D = 2.1-5$) where the values of C_{Df} and C_{Lf} are extensively high, $\sim$2.35 and 1.58 times the single cylinder values. The high values of C_{Df} and C_{Lf} are ascribed to vortex and cylinder and vortex and shear layer interactions, respectively. Both shear layer or wake and cylinder, and boundary layer and cylinder interactions weaken C_{Df}, C_{Lf}, and flow unsteadiness. While the former interaction stabilizes the wake or shear layers, the latter one forms a separation bubble, delays boundary layer separation, or causes reattachment. The separation bubble formation results in maximum repulsive C_L of +0.86 at $|\alpha| = 135^\circ$, $T/D = 0.1-0.2$. Maximum C_D of 1.75 acts on the cylinders in the regime of $|\alpha| = 90^\circ$, $T/D = 2.2-2.6$ (regime 6) caused by a strong vortex and vortex interaction, which is $\sim$1.56 times the single cylinder value.

ACKNOWLEDGMENTS

M.M.A. wishes to acknowledge support given to him by NRF through Grant No. A0U368, by UP RDP through Grant No. AOT366, and by UP Research and Innovation Support through Grant No. AOS971.

[1] M. M. Zdravkovich, J. Fluids Struct. **1**, 239 (1987).
[2] D. Sumner, S. J. Price, and M. P. Paidoussis, J. Fluid Mech. **411**, 263 (2000).
[3] Z. Gu and T. Sun, J. Wind Eng. Indust. Aerodyn. **80**, 287 (1999).
[4] T. Karasudani and M. Funakoshi, Fluid Dyn. Res. **14**, 331 (1994).
[5] O. Inoue and T. Yamazaki, Fluid Dyn. Res. **25**, 1 (1999).
[6] P. Vorobieff, D. Georgeiev, and M. S. Ingber, Phys. Fluids **14**, 53 (2002).
[7] E. Hori, *Proceedings of the Ninth Japan National Congress for Applied Mechanics, paper III-11*, 1959, pp. 231–234 (unpublished).
[8] K. R. Cooper, National Aeronautical Establishment report No. LTR-LA-115, Ottawa, Canada, 1973 (unpublished).
[9] J. Price, Aeronautical Quarterly **26**, 154 (1976).
[10] M. M. Zdravkovich and D. L. Pridden, J. Indust. Aerodyn. **2**, 255 (1977).
[11] M. M. Zdravkovich, J. Wind Eng. Indust. Aerodyn. **6**, 59 (1980).
[12] A. Bokaian and F. Geoola, J. Fluid Mech. **146**, 383 (1984).
[13] S. J. Price and M. P. Paidoussis, J. Wind Eng. Indust. Aerodyn. **17**, 329 (1984).
[14] M. Abdulhadi, J. Wind Eng. Indust. Aerodyn. **21**, 101 (1985).
[15] N. W. M. Ko and P. T. Y. Wong, J. Wind Eng. Indust. Aerodyn. **41–44**, 563 (1992).
[16] Z. F. Gu, T. F. Sun, D. X. He, and L. L. Zhang, J. Wind Eng. Indust. Aerodyn. **49**, 379 (1993).
[17] R. L. Wardlaw and K. R. Cooper, National Research Council of Canada Report No. LTR-LA-117, 1973 (unpublished).
[18] M. M. Alam, M. Moriya, and H. Sakamoto, J. Fluids Struct. **18**, 325 (2003).
[19] M. M. Alam, M. Moriya, K. Takai, and H. Sakamoto, J. Wind Eng. Indust. Aerodyn. **91**, 139 (2003).
[20] M. M. Alam, H. Sakamoto, and Y. Zhou, J. Fluids Struct. **21**, 363 (2005).
[21] M. M. Zdravkovich, ASME J. Fluids Eng. **199**, 618 (1977).
[22] D. S. K. Ting, D. J. Wang, S. J. Price, and M. P. Paidoussis, J. Fluids Struct. **12**, 259 (1998).
[23] K. Kamemoto, Bull. Jpn. Soc. Mech. Eng. **19**, 283 (1976).
[24] M. Kiya, M. Arie, H. Tamura, and H. Mori, J. Fluids Eng. **102**, 166 (1980).
[25] J. A. Jendrzejczyk and S. S. Chen, in *Proceedings of the International Conference on Flow-Induced Vibration 1986* (ASME, New York, 1986), PVP Vol. 104, pp. 1–13.
[26] T. Igarashi, Bull. Jpn. Soc. Mech. Eng. **24**, 323 (1981).
[27] T. Igarashi, Bull. Jpn. Soc. Mech. Eng. **27**, 2380 (1984).
[28] H. Zhang and W. H. Melbourne, J. Wind Eng. Indust. Aerodyn. **41–44**, 589 (1992).
[29] T. Nishimura, Y. Ohori, and Y. Kawamura, Int. Chemical Engg. **26**, 123 (1986).
[30] P. Le Gal, M. P. Chauve, R. Lima, and J. Rezende, Phys. Rev. A **41**, 4566 (1990).
[31] I. Peschard and P. Le Gal, Phys. Rev. Lett. **77**, 3122 (1996).
[32] C. H. K. Williamson, J. Fluid Mech. **159**, 1 (1985).
[33] G. S. West and C. J. Apelt, J. Fluid Mech. **14**, 361 (1982).
[34] G. S. West and C. J. Apelt, J. Fluids Struct. **7**, 227 (1993).
[35] S. Szepessy and P. W. Bearman, J. Fluid Mech. **234**, 191 (1992)
[36] H. Sakamoto and S. Oiwake, J. Fluids Eng. **106**, 160 (1984).
[37] H. Sakamoto, H. Haniu, Y. Obata, and S. Matubara, JSME Int. J., Ser. B **37**, 369 (1994).
[38] C. H. K. Williamson, J. Fluid Mech. **328**, 345 (1996).
[39] M. M. Alam and Y. Zhou, J. Fluid Mech. **589**, 261 (2007).
[40] M. M. Alam and Y. Zhou, Phys. Rev. E **78**, 036320 (2008).
[41] V. Kolar, D. A. Lyn, and W. Rodi, J. Fluid Mech. **346**, 201 (1997).
[42] J. R. Meneghini, F. Satara, C. L. R. Siqueira, and J. A. Ferrari, J. Fluids Struct. **15**, 327 (2001).
[43] M. M. Alam, Y. Zhou, and X. W. Wang, J. Fluid Mech. **669**, 432 (2010).
[44] M. M. Alam and H. Sakamoto, J. Fluids Struct. **20**, 425 (2005).
[45] I. Gursul and D. Rockwell, J. Fluid Mech. **211**, 211 (1990).
[46] M. M. Zdravkovich, J. Wind Eng. Indust. Aerodyn. **7**, 145 (1981).
[47] M. M. Alam, H. Sakamoto, and Y. Zhou, J. Wind Eng. Indust. Aerodyn. **94**, 525 (2006).
[48] D. F. James and Q. S. Truong, Proc. ASCE J. Eng. Mech. **98**, (EM6), 1573 (1972).
[49] M. M. Alam, Y. Zhou, Z. M. Zhao, O. Flamand, and O. Buojard, Int. J. Heat and Fluid Flow **31**, 845 (2010).
[50] H. Sakamoto, K. Tan, and H. Haniu, J. Fluids Eng. **113**, 183 (1991).
[51] M. M. Alam, H. Sakamoto, and M. Moriya, J. Fluids Struct. **18**, 347 (2003).
[52] B. J. Knell, Natl. Phys. Lab. (UK), Aero. report No. 1297 (1969).
[53] P. W. Bearman, J. Fluid Mech. **21**, 241 (1965).
[54] I. Igarashi and S. Itoh, J. Fluids Eng. **59**, 3701 (1993).
[55] H. Sakamoto, N. Takeuchi, H. Haniu, and K. J. Tan, J. Fluids Eng. **119**, 506 (1997).
[56] M. M. Alam and Y. Zhou, J. Fluids Struct. **23**, 799 (2007).